CEAS EuroGNC 2019
"Conference on Guidance, Navigation and Control"
3-5 April 2019 @ Politecnico di Milano, Milan, Italy.

CEAS-GNC-2019-014

Glide path generation with regard to wind misestimations.

Marius Klein, Andreas Klos and Wolfram Schiffmann.

Abstract In an emergency situation with total loss of thrust the pilot is forced to perform an emergency landing under difficult conditions. The potential energy of the aircrafts altitude can be converted into kinetic energy to move a certain distance over ground. In the best case this enables the aircraft to reach a suitable landing field at a proper altitude and direction. In a previous paper we presented a fast and non-iterativ algorithm to calculate glide pathes to a moving target in the wind frame. In this paper we discuss the necessity of precise wind prediction and extend the algorithm to be robust towards misestimation of wind force or wind direction. Furthermore, we consider a selection strategy in case that more than one valid glide path is feasible. Here, the strategy selects the trajectory that offers an alternative path as least as possible and is also robust against of the wind misestimation.

Marius Klein
Faculty of Mathematics and Computer Science, FernUniversität in Hagen, Germany, e-mail: marius.klein@fernuni-hagen.de

Andreas Klos
Faculty of Mathematics and Computer Science, FernUniversität in Hagen, Germany, e-mail: andreas.klos@fernuni-hagen.de

Wolfram Schiffmann
Faculty of Mathematics and Computer Science, FernUniversität in Hagen, Germany, e-mail: wolfram.schiffmann@fernuni-hagen.de

1 Introduction

Forced landings of an aircraft can be caused by total or partial engine-failures, fire or smoke on board etc. In this article, we consider aircrafts with a total loss of thrust caused by an engine-failure. In such situations, the pilot is forced to conduct an emergency landing which require fast, intuitive and proper decision. The support of the pilot during such extreme situations is considered as major issue. Moreover, the importance of an Emergency Landing Assistant (ELA) gained much attention because of the US Airways Flight 1549 in 2009. Short after take-off a bird-strike occurred and both engines of the Airbus A320 failed so that the pilot was forced to perform an emergency landing. In this situation, it is desirable to have a supporting assistant system which takes over the guidance to the most suitable runway within reach.

In this paper, we present an extended version of ELA proposed in [1] which is capable to compute a wind-aware flight path from the current configuration of the aircraft (position, heading, speed) to an emergency landing field. Thereby, the extended version of ELA is more robust against wind misestimations of wind force or direction. A database with possible emergency landing fields is assumed to be available. These are published airfields with paved runways in the best case. The corresponding geodata of those airfields is available worldwide. In another paper of our group we presented a method to identify those emergency landing fields, [2].

Frequently, Dubins curves are used to calculate the path between two configurations of a kinematic model. Dubins curves [3] were introduced in 1957 and are used for the computation of the shortest, possible path between two car configurations. To compute flight paths for aircrafts these originally two-dimensional approaches have been extended by the third dimension in recent years [4].

During the glide along the flight path the excess altitude is used to compensate the missing thrust in order to reach an emergency landing field. Simultaneously, most of the excess altitude should be consumed on the glide path so that the aircraft reaches the beginning of the emergency landing field at an appropriate altitude of a few meters above ground and with a suitable landing configuration (speed and runway).

Unfortunately, previous research on Dubins curves was restricted to windless situations. Obviously, the influence of the wind has to be considered, especially, if the wind contributes to a negligible share of the aircraft's velocity. In order to take the wind into account, methods have been developed that observe the aircraft from the earth (frame) which causes trochoidal curves [5]. Thereby, a start trochoid is applied at the emergency configuration. At the runway configuration a final trochoid is fitted. Both trochoids have to be connected by a tangent. However, the trochoid method has three serious disadvantages: First, the altitude loss during the gliding path can only be adopted by the variation of the trochoid radii and/or the number of turns. Second, the calculation of the tangent is complex and only an approximated solution can be found. Third, it is restricted to a two circle approach and uniform wind conditions during the glide.

In this paper, we address the wind problem by an elementary but efficient solution that can be used with any type of approach path which offers more flexibility, even though the aircraft is gliding through layers with changing wind patterns. Nevertheless, we only consider a constant wind vector in this paper.

The basic idea of our technique is to perform the calculations in the wind frame and transform the resulting flight path back to the earth frame. This method avoids the complicated computations of fitting the trochoids to the start and final configurations as well as the tangent between both trochoids. Instead we move the destination (e. g. runway threshold) opposite to the wind direction into the wind frame . The subsequent path calculations are performed as in the windless case and thus the complexity of the computation can be reduced dramatically.

The wind and earth frame are congruent in the windless case. Under the influence of wind, the wind frame moves opposite to the wind vector. The vector of the displacement is computed by the wind vector and the time elapsed during consumption of the excess altitude. If the duration of the approach can be estimated, the moved position of the target configuration can be calculated. Fortunately, for co-rotating Dubins curves it is possible to give a pretty precise estimate of the approach time. Thus, we can easily calculate a wind-aware solution by moving the target configuration opposite to the wind. For the moved target, we can proceed to determine the Dubins' paths like in the windless case. Note that this approach can be applied only to path planning methods as long as there is an estimation for the gliding time. In order to obtain a trajectory in the earth frame we can transform the wind frame solution by moving sampling points alongside the wind vector for the corresponding time expired since the start of the approach.

To make the flight path more robust against wind, we integrated an iterative calculation which adds full circles to the trajectory. These circles were attached to the final approach and so the flight path leads closer to the target landing position. Thus, misestimations of the wind direction or force are less influential.

The remaining paper is organized as follows. In Sec. two we give an overview of the related work. In the third and fourth Sec. we introduce the glide path calculation and compare the standard algorithm with the extended iterative calculation. Afterwards, in Sec. 5 our simulation results for misestimation of wind direction or wind force are examined and evaluated. In the last Sec., we conclude the proposed results and give an outlook on our future work.

2 Related Work

The calculation of flight paths under emergency conditionshas proven as a non-trivial problem. Researchers have developed several approaches to determine an optimal flight path with various kinds of targets and conditions.

These include genetic algorithms like proposed in [6] which is focused on the avoidance of cylindrical obstacles in the horizontal plane without the consideration of the influence of wind. Thereby, a random- and an elitism-based immigrant

scheme is combined adaptively. Liu et al. proposed another genetic algorithm that is capable to determine a three-dimensional flight path under the assumption of no wind [7]. The developed algorithm is basically inspired by the biological immune system and is able to avoid obstacles.

Moreover, various swarm based algorithms are applied to enable path planning for dynamic models which includes the specialized utilization in flight path planning for an aircraft. In [8] a representative swarm algorithm is proposed which enables three-dimensional path planning for unmanned aerial vehicles (UAVs). This algorithm is capable to avoid obstacles. Unfortunately, this approach doesn't consider the influence of wind during the flight path computations. But this is crucial, especially for light weighted UAVs.

The Rapidly-exploring Random Tree (RRT) method for motion planning was introduced in 1998 by LaValle[9]. Since then, this concept of path planning was often applied to various dynamic vehicle models like robots as proposed by Pepy et al. [10]. Levora et al. introduced an informed RRT algorithm which is focused on the two-dimensional motion planning for non-linear, non-holonomic systems with an unknown inverse kinematic description[11]. However, these approaches as well as the presented genetic algorithms omit the path planning under wind impact.

Furthermore, the flight path planning is considered as a higher-dimensional optimal control problem. Adler et al. proposed an algorithm based on motion primitives which enables the calculation of a six-dimensional optimal control problem. This approach results in an energy efficient solution and reduces the planning problem to a graph-search problem under the restricted conditions of calm air[12].

Another key technique in the flight path planning field are the Dubins curves.This method was introduced by Lester E. Dubins in 1957 and has become an essential research area in the field of path planning [3]. Dubins curves were initially developed for two-dimensional path planning for car models with the objective to reach a target from a starting position within the shortest path. This path planning approach consists of the three motion primitives listed in Tab. 1.

Table 1 The three motion primitives and their meaning.

Symbol	Description
S	Straight ahead
R	Closest possible turn to the right
L	Closest possible turn to the left

Dubins has demonstrated that a combination of only three motion primitives is necessary to calculate the shortest path between two car configurations [3]. Besides, Dubins showed that only six concatenations of the introduced motion primitives result in a possible optima. In Fig. 1 the following four configurations are illustrated.

$$\{\text{LSL, RSR, LSR, RSL}\}$$

Therein, the previously mentioned motion primitives for the four flight paths are shown. The point S denotes the start position and the arrow attached to S is the

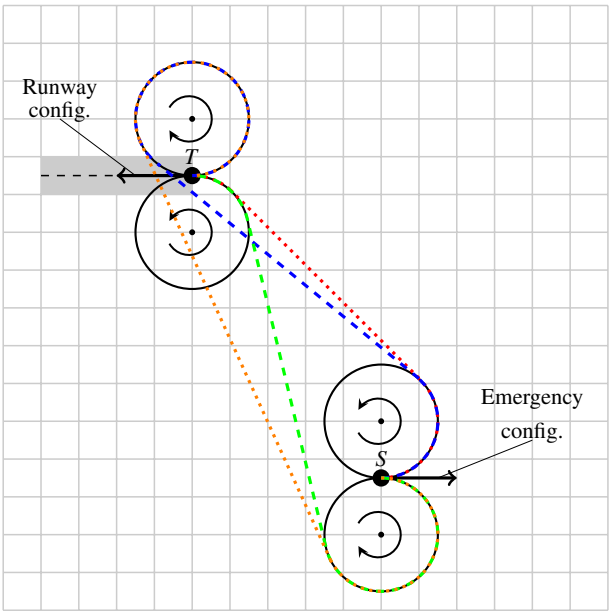

Fig. 1 Considered flight path opportunities to reach the runway from a certain position.

heading of the aircraft. Furthermore, the runway is illustrated as gray rectangle in the top on the left-hand side. The corresponding direction of the runway is denoted by the arrow attached to our target point (runway threshold) T.

Initially, Dubins curves were applied for path planning of cars. Later, the car was exchanged by an aircraft and the technique was adopted with the goal to support three-dimensional path planning [13]. In [14] a standard autopilot with low-level controller based on Dubins curves was developed. The main objective was to maintain the aircraft undamaged during the flight instead of reaching a certain target within minimum distance or flight time.

The considered car model was replaced by an aircraft model to facilitate three-dimensional path planning. The configuration of the aircraft can be expressed as $c = (x, y, z, \psi, \phi, \theta)$, where the vector (x, y, z) describes the three-dimensional position, ψ represents the heading, ϕ the bank angle, and θ the pitch angle.

First, the turning radius is calculated using Eq. 1, where r is the radius of the initial and the final turn, V_a denotes the speed of the aircraft, g represents the gravitational acceleration (9.80665 $\frac{m}{s^2}$), and ϕ is the bank angle that can differ in the sign[13].

$$r = \frac{V_a^2}{g \cdot tan(\phi)} \tag{1}$$

The pilot has to fly the turn with bank angle ϕ to realize the radius r. For simplification purposes the turnings are considered as circles as shown in Fig. 1. The outer

and inner tangents (dotted and dashed straight line segments) are fitted to the four circles[13]. The inner tangents are computed for the RSLS and the LSRS approach. The outer tangents are calculated for the LSLS and the RSRS approach. Only four tangents in combination with the turnings can facilitate the desired final heading of the aircraft.

Unfortunately, this new technique still neglects the influence of wind. Nevertheless, the consideration of the wind effect is a crucial issue. Hence, Warren and Coombes et al. investigate the flight path planning problem influenced by wind in [15] and in [16]. The circle-pattern of the Dubins curves is replaced by a trochoid pattern. In the earth frame a constant wind causes a distortion of circles flown in the wind frame to a so called trochoids. Schopferer et al. have introduced a quite similar approach based on the Dubins curves and the trochoid pattern. This algorithm combines the Dubins curves algorithm used for the calculation of the flight path in the horizontal plane with a bang-bang control strategy to facilitate three-dimensional flight path planning in a constant wind [17]. Izuta et al. have presented a flight path planning algorithm to adjust the length of the final approach with the goal to improve the reachability in a forced landing. Unfortunately, they assume the windless case and if they increase or decrease the final approach, changes in the length of the flight path during both turns are left unconsidered [18]. This may be interesting in the case of two contrary rotating circles.

A fixed final approach for the flight path planning was examined by Coombes et al. [16] and was further refined in the PhD thesis of Coombes [5]. The improved technique takes a constant wind into account.

Moreover, McGee et al. describe an optimal path planning algorithm in a constant wind based on the Minimum Principle. The used algorithm re-expresses the influence of the wind as the problem of finding the optimal path planning from an initial position and orientation with no wind to a final position and orientation of a moving virtual target. However, the objective of the developed algorithm was the planning of a flight path with a minimum length[19].

We propose a efficient method based on Dubins curves to facilitate a three-dimensional wind-robust flight path planning in constant wind. This approach takes the contribution of the wind into account by performing the calculations in the wind frame. Thus, the transformation into the earth frame and the complex fitting of a straight line segment between two trochoids can be avoided. In contrast to the Dubins curves the intention of our technique is to reach the landing field at an appropriate altitude by adjusting the length of the final approach. Furthermore, our algorithm offers the possibility to add full circles to the trajectory and generate a flight path close to the target landing field. In this way, the route is robust with regard to misestimations of wind force and wind direction.

3 Fast and wind-aware glide path planning

This subsection shows how an approach path can be calculated directly for two cases without the necessity of an iterative procedure. The following parameters are required as input for the algorithm: coordinates and heading of the aircraft and the runway, the elevation difference between aircraft and runway, the radius of both circles, the optimal speeds in curve and straight-ahead flight and the corresponding glide ratios in the straight-ahead and curve segments. The glide ratio indicates the amount of altitude an aircraft loses on a predetermined distance. For example, a glide ratio of 0.1 indicates that an aircraft loses 1 meter of altitude by gliding a distance of 10 meters. The environmental parameters are wind velocity and direction.

To simplify the calculation, some preparatory work has to be done. First, the coordinates (latitude, longitude) of the runway and the aircraft are transformed from the geographical coordinate system into a Cartesian coordinate system. After the conversion, the origin of the Cartesian coordinate system denotes the target point of the approach path.

In the next step, the coordinate system is rotated around the origin such that the approach direction of the runway is in the direction of the positive x-axis. We also need to pay attention that the heading of the aircraft and the direction of the wind vector must be likewise rotated. Since a runway has two approach directions, we perform the following calculations for both of them. For the right side approach we implement the calculation and can compute paths for any start configuration. For the left side approach, we rotate the coordinate system by 180° and perform the same calculation applied to the right side approach. Afterwards, the computed path has to be rotated back. The basic computation is identically for both sides as presented in the following.

The initial situation after the rotation can be seen in Fig. 2. The point S denotes the converted and rotated aircraft starting position of the path. The point T is the target and is located in the origin of the coordinate system. By assuming windless environmental conditions, the point T corresponds to the destination point in the wind as well as the earth frame. Otherwise, the point T is moved towards the wind direction with the magnitude of the wind vector over the approximated approach time. The calculation of the co-rotating circle approach is the same in both cases. The initial heading of the aircraft is represented by a black arrow. The approach direction of the runway is aligned to the positive x-axis. In addition to that, the co-rotating approach paths are shown with left-turning circle segments – solid – and right-turning circle segments – dotted – which are located on the start-circles I_1, I_2 and end-circles O_1, O_2.

The next step is to summarize some cases like shown in Fig. 3. A RSRS approach with starting point (x_0, y_0) corresponds to the LSLS approach with starting point $(x_0, -y_0)$, mirrored at the x-axis. This procedure is also valid for the reversed case. The current considered RSRS approach with the starting point S is mirrored at the x-axis. Thus, the following calculation can be considered as an LSLS approach with the starting point S'. Finally, the computed path has to be mirrored back. In the same way, the calculation can be done for the other side of the runway. In this case the

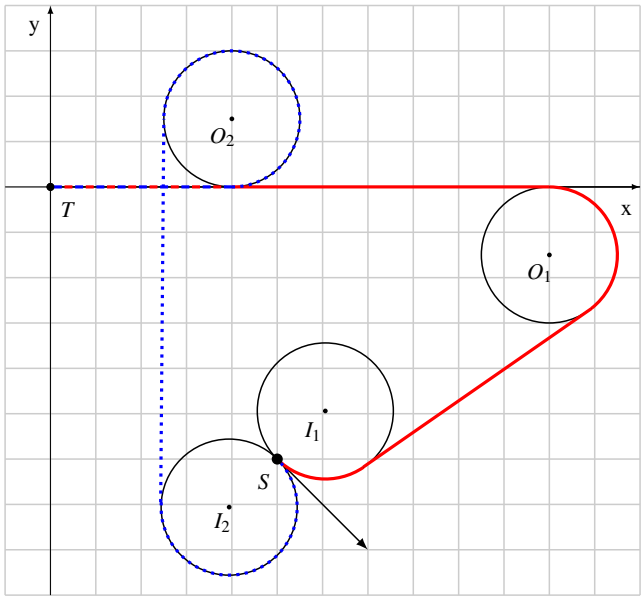

Fig. 2 Schematic approach paths for LSLS and RSRS approaches.

start configuration of the aircraft is mirrored at the y-axis. In the further work we show the calculation of the LSLS approach from the right side. The LSLS approach from the left side and the RSRS approaches from right and left side of the origin can be derived from LSLS right approach by mirroring as previously explained.

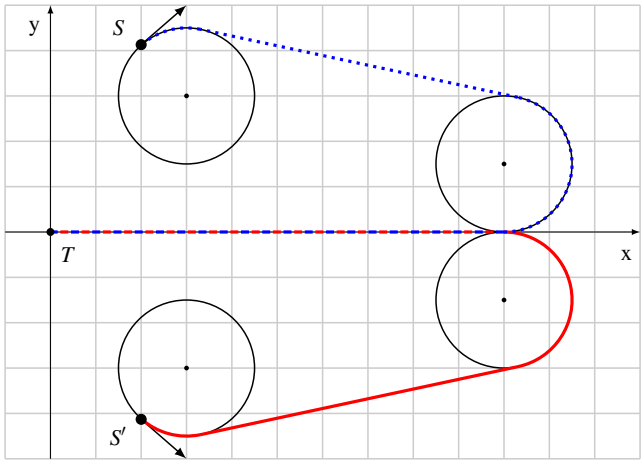

Fig. 3 Mirroring at the x-axis and converting from RSRS-approach to LSLS-approach.

The initial configuration is shown in Fig. 4 as an example for a LSLS approach. The path is subdivided into four segments: an in-segment d_I, a tangent-segment d_T, an out-segment d_O and an end-segment d_E. For a RSRS approach, the partitioning is similar.

The coordinates of the start-circle are calculated with the heading of the aircraft ψ and the given radius r of the circle. The point (x_1, y_1) is located on the left-side orthogonal to the heading direction of the aircraft with distance r. In the case of a right turning in-circle, the point on the right-side orthogonal to ψ with distance r is determined.

For a left-turning out-circle, the y-value equals $-r$, so that the circle touches the x-axis from below. For a right-turning out-circle the y-value is r so that the circle touches the y-axis from above.

The distance between the origin and the out-circle in x-direction – in the following denoted by d_E – can be varied to adjust the length of the final approach. Thus, the difference in altitude between the aircraft and the runway can be reduced. The different glide ratios in turning s_C and straight flight segments s must be considered as shown in Eq. 2.

$$\Delta_H = (d_T + d_E) \cdot s + (d_I + d_O) \cdot s_C \quad . \tag{2}$$

The total altitude difference between starting and target configuration Δ_H, corresponds to the sum of the reduced altitudes in the four segments. Thereby, d_E can be calculated directly from this equation.

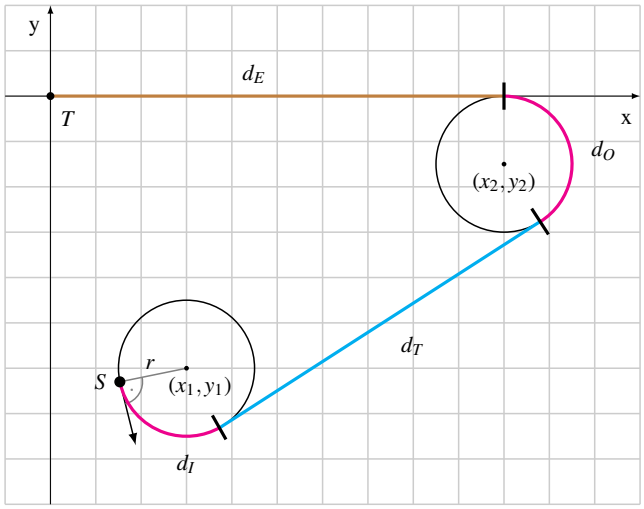

Fig. 4 Approach segmentation for the LSLS approach.

If the circle segments rotate in the same direction, the sum of the segments $(d_I + d_O)$ can be derived from the total flown angle β and the radius r. Thereby, β is

calculated from the aircraft heading ψ and the runway direction (here 270°). For an LSLS approach with $90° \leq \psi < 270°$ the value is $\beta = 90° + \psi$. A case distinction has to be performed for a start configuration between $270° \leq \psi < 90°$. If d_E is negative or so large that the out-circle is too far on the right side of the runway threshold right an additional rotation of 360° has to be executed. The total covered angle sums up to $\beta = 360° + 90° + \psi$. For a RSRS approach the same applies with slightly difference. In this case the angle is located at the other direction from the heading but β can be calculated.

For a known angle β, the sum of the circular segments d_C is computed as shown in Eq. 3.

$$d_C = d_I + d_O = 2 \cdot r \cdot \pi \cdot \frac{\beta}{360°} \quad . \tag{3}$$

Afterwards, the length of the tangent segment d_T is a function of d_E as described by Eq. 4.

$$d_T = \sqrt{(y_2 - y_1)^2 + (d_E - x_1)^2} \quad . \tag{4}$$

Subsequently, Eq. 3 and 4 are substituted in Eq. 2. This results in Eq. 5.

$$\Delta_H = \sqrt{(y_2 - y_1)^2 + (d_E - x_1)^2} \cdot s + d_E \cdot s + d_C \cdot s_C \quad . \tag{5}$$

Finally, Eq. 5 is solved for d_E which is shown in Eq. 6.

$$d_E = \frac{-\Delta_H^2 + (s \cdot x_1)^2 + 2 \cdot \Delta_H \cdot d_C \cdot s_C - (d_C \cdot s_C)^2 + (s \cdot y_1)^2 - 2 \cdot s^2 \cdot y_1 \cdot y_2 + (s \cdot y_2)^2}{2 \cdot s \cdot (-\Delta_H + s \cdot x_1 + d_C \cdot s_C)} \quad . \tag{6}$$

Using Eq. 6, the final approach length d_E of the end-circle can be precisely calculated. The resulting approach reduces the altitude of the aircraft accurately. Note that d_E should be positive, otherwise the length of the approach path is too long for the available altitude of the aircraft and the runway is not reachable. A value of 0 implies that the approach can still be flown with the current altitude but the end-circle touches the target point. Furthermore, the case distinction regarding to the calculation of β can lead to certain altitudes which cannot be eliminated. In this case, it may be possible that the extended approach becomes too long. A solution of this problem includes other alternative approach paths, e. g. an RSLS or an LSRS approach. By combining these approaches it is ensured that at least one valid approach path is obtained from a certain minimum altitude.

4 Wind robust glide pathes with fault tolerance to misestimations

An unfavorable characteristic of the presented algorithm in Sec. 3, which is based on Dubins curves with extended final approach, is the strictly positive correlation

between d_E and Δ_H. For high altitudes Δ_H the end circle is positioned comparative far off the target position. Therefore, the calculated trajectory initially leads away from the target which is problematically in two ways. At first, it may seem contradictory for the pilot if the route leads away from the destination rather than towards it. The second problem is the necessity for a good estimate of wind parameters, namely wind force and wind direction. For small aircrafts, these parameters must be estimated and can contain inaccuracies. In addition to that, only the local wind situation of the aircraft is considered but the parameters can change dynamically during the flight. Then, the calculated route in the earth frame differs from the actual flown route to reach the destination. If the pilot flies the route calculated with wrong wind parameters, he will end up at a point where even a recalculation with the correct parameters will not be possible. At this point, further named the Point Of No Return (PONR), the target position can no longer be reached.

The aim of the wind-robust extension of the algorithm is to achieve a PONR on the trajectory as late as possible. In this case, the pilot has the maximum time to correct errors resulting from misestimation of wind parameters. Instead of eliminating the remaining altitude by extending the final approach it can be reduced by flying additional full circles. Therefore, the original algorithm is extended by an iterative procedure with a while loop which increases d_C from Eq. 3 by a full circle as long as a valid route can be calculated. The value of d_C to be added is shown in Eq. 7,

$$d_C(n) = d_C(n-1) + 2 \cdot r \cdot \pi \cdot \frac{360^\circ}{360^\circ} = d_C(n-1) + 2 \cdot r \cdot \pi \quad . \tag{7}$$

In Fig. 5, a calculated route is shown without algorithm extension. The starting position, represented as an airplane, is nearly 1.5 km away from the target position, represented as the black runway. The glide ratio is 0.1 and the altitude 700 m. The gray route is the calculated route with a moving target in the wind frame. The black trajectory is the resulting route in the earth frame.

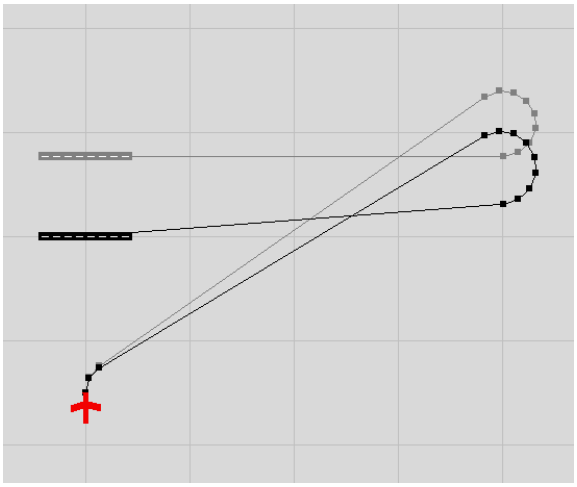

Fig. 5 Algorithm without full circle extension.

In Fig. 6, the calculated route with the same situation and with wind robust extension of the algorithm is shown. In this case, two additional full circles can be flown which reduces the final approach to eliminate the remaining altitude. The new circles are attached to the target position so that the resulting trajectory is generated as close as possible to the destination point. Probably, these glide paths are more difficult to fly because the final turn ends directly at the runway threshold but this is neglected. Otherwise, the circles could also be appended at any other point of the route in the wind frame, e. g. the middle of the final approach. In Sec. 5 we will show that the full circle method shifts the average PONR significantly to the end of the trajectory.

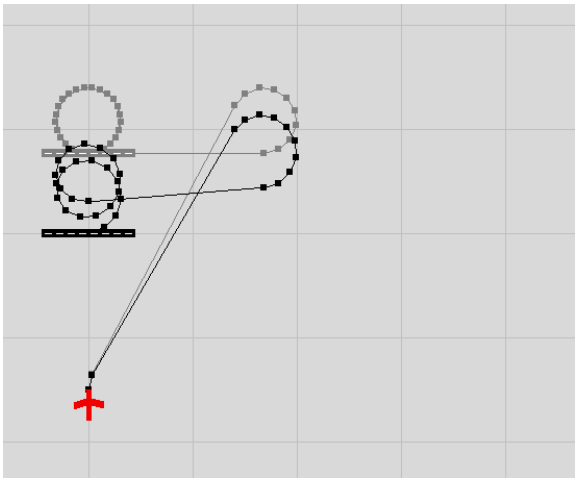

Fig. 6 Algorithm with full circle extension.

5 Results

In this section, we consider the two route types with regard to their tolerance to misestimation of the wind force or direction. The parameters are measured by a sensorsystem in the aircraft and are assumed to be constant during the entire flight. Furthermore, we assume that the measured are error-prone and differ from the real wind parameters. Thus, the calculated route differs from the actual route to be flown to reach the target position. In the further simulation we assume a constant misestimation of one parameter, either wind force *or* direction. A volatile misestimation over time or misestimations of both parameters at the same time are not considered.

To determine the PONR, the trajectory calculated with misestimated parameters in the earth frame is divided into 100 equidistant points. As mentioned in Sec. 4, the PONR depicts the waypoint, where even with correct wind parameters no new valid route can be found. An iterativ method loops the array of the 100 points and tries to

recalculate a valid route with the correct wind parameters. The last point for which this is possible is the PONR and is be indicated as the position on the trajectory in percentage.

In our previous research [1] we have presented a simulator which is capable to multivariate a parameter range of possible flight paths with variable starting configurations and a fixed target position (runway threshold). For further studies, we enhanced the simulator to determine the PONR of every calculated path. To achieve comprehensive results, we need to provide reasonable step sizes and bounds to our simulation software for the following parameters:

- X and Y grid dimension (in m),
- initial aircraft altitude (in m) and heading (in degree), and
- wind velocity (in $\frac{km}{h}$) and direction (in degree).

The used values are parametrized as shown in Tab. 2.

Table 2 Grid values of the simulator.

Parameter	**From**	**To**	**Step size**
Grid dimension X $[m]$	$-5\,000$	$5\,000$	200
Grid dimension Y $[m]$	$-5\,000$	$5\,000$	200
Initial aircraft altitude $[m]$	100	2000	50
Initial aircraft heading $[^\circ]$	0	315	45
Wind velocity $[\frac{km}{h}]$	0	80	20
Wind direction $[^\circ]$	0	315	45

Furthermore, we need to provide the following aircraft model specific parameter to our simulation software:

- Aircraft velocity on straight flight segments and during turnings ($\frac{km}{h}$),
- glide ratio on straight flight segment and during turnings, and
- turning radius (m).

As in [1], we selected a Cessna 182 because this aircraft is widely used and well known in General Aviation (GA). The related values are shown in Tab. 3.

Table 3 Used values of the Cessna 182 aircraft model.

Parameter	**Value**
Aircraft velocity straight flight $[\frac{km}{h}]$	125.53
Aircraft velocity in turning flight $[\frac{km}{h}]$	128.84
Glide ratio straight flight	0.086
Glide ratio in turning flight	0.089
Radius $[m]$	487.47

We consider four misestimations each for the wind force and direction. For example, a misestimation of +5 km/h means, that the predicted wind force is 8 km/h

while the real wind force is 3 km/h. In the same way the misestimations of the wind direction are denoted. In Tab. 4 the results of the simulations are listed. For each misestimation and route types (with extended final approach and with full circle approach) the *average* PONRs are listed. It can be seen, that the full circle approach shifted the PONR significantly backwards on the trajectory. For misestimations of the wind force the PONR changes from 66%–74% to 79%–85%. Likewise, for the wind direction it changes from 81%–85% to 90%–92%. So, in the average case the pilot has more time to recognize the error and recalculate the route with the correct wind parameters. Otherwise, it must be considerd that the route type with full circles is more difficult to fly as mentioned in Sec. 4.

Table 4 Average position of the PONR.

misestimation (wind force) +10 km/h with extended final approach	74%
misestimation (wind force) +5 km/h with extended final approach	69%
misestimation (wind force) -5 km/h with extended final approach	67%
misestimation (wind force) -10 km/h with extended final approach	66%
misestimation (wind direction) -20 $^\circ$ with extended final approach	81%
misestimation (wind direction) -10 $^\circ$ with extended final approach	85%
misestimation (wind direction) +10 $^\circ$ with extended final approach	85%
misestimation (wind direction) +20 $^\circ$ with extended final approach	81%
misestimation (wind force) -10 km/h with full circle approach	85%
misestimation (wind force) -5 km/h with full circle extension	83%
misestimation (wind force) +5 km/h with full circle extension	81%
misestimation (wind force) +10 km/h with full circle extension	79%
misestimation (wind direction) -20 $^\circ$ with full circle approach	90%
misestimation (wind direction) -10 $^\circ$ with full circle approach	92%
misestimation (wind direction) +10 $^\circ$ with full circle approach	92%
misestimation (wind direction) +20 $^\circ$ with full circle approach	90%

6 Conclusion and future work

In this paper, we presented an enhancement of our route calculation algorithm with regard to misestimation of wind force or wind direction. We showed, that paths with additional full circles instead of an extended final approach are closer to the target position and gives the pilot more time to react to errors by misestimation. The Point Of No Return is significantly shifted backwards on the trajectory.

In future work, we will implement the algorithm in an android application for testing it in flight simulators or real aircrafts. Furthermore, we consider the necessity of a suitable human-machine interface for emergency situations in aircrafts. Appart from that, we develop an autopilot for small UAVs that can perform autonomous landing in an emergency situation by using ELA.

References

[1] M. Klein, A. Klos, J. Lenhardt, and W. Schiffmann, "Moving target approach for wind-aware flight path generation," *International Journal of Networking and Computing*, vol. 8, no. 2, pp. 1–16, 2018.

[2] F. Eckstein, B. Wittich, and W. Schiffmann, "Emergency landing field recognition based on elevation data using parallel processing," in *Proceedings of the Digital Avionics Systems Conference*, AIAA, Ed., 2018.

[3] L. E. Dubins, "On Curves of Minimal Length with a Constraint on Average Curvature, and with Prescribed Initial and Terminal Positions and Tangents," *American Journal of Mathematics*, vol. 79, pp. 497–516, 1957, ISSN: 0002-9327. DOI: 10.2307/2372560. [Online]. Available: http://www.jstor.org/stable/10.2307/2372560.

[4] M. Owen, R. W. Beard, and T. W. McLain, "Implementing dubins airplane paths on fixed-wing uavs," *Handbook of Unmanned Aerial Vehicles*, pp. 1677–1701, 2015. DOI: 10.1007/978-90-481-9707-1{_}120. [Online]. Available: http://scholarsarchive.byu.edu/cgi/viewcontent.cgi?article=2926%7B%5C&%7Dcontext=facpub.

[5] M. Coombes, ""Landing site reachability and decision making for UAS forced landings Making for UAS Forced Landings"," PhD thesis, Loughborough University, 2016.

[6] X. Fu and X. Gao, "Genetic algorithm with adaptive immigrants for dynamic flight path planning," in *2010 IEEE Int. Con. on Intelligent Computing and Intelligent Systems*, vol. 1, Oct. 2010, pp. 630–634. DOI: 10.1109/ICICISYS.2010.5658510.

[7] L. Liu and S. Zhang, "Three-dimensional flight path planning by artificial immune algorithm," *Natural Computation, 6th Int. Conf.*, pp. 2876–2880, 2010. DOI: 10.1109/ICNC.2010.5584119.

[8] Y. Cai, H. Zhao, M. Li, and H. Huang, "3D real-time path planning based on cognitive behavior optimization algorithm for UAV with TLP model," in *Cluster Computing*, 2018.

[9] S. M. Lavalle, "Rapidly-exploring random trees: A new tool for path planning," 1998.

[10] R. Pepy, A. Lambert, and H. Mounier, "Path Planning using a Dynamic Vehicle Model," *2006 2nd Int. Conf. on Information and Communication Technologies*, vol. 1, 2006. DOI: 10.1109/ICTTA.2006.1684472.

[11] T. Levora, O. Bruna, and P. Pavel, "Path planning for ultralights under emergency," in *29th Congress of the International Council of the Aeronautical Sciences*, St. Petersburg, Russia, 2014, pp. 1–7. [Online]. Available: http://www.icas.org/ICAS%7B%5C_%7DARCHIVE/ICAS2014/data/papers/2014%7B%5C_%7D0882%7B%5C_%7Dpaper.pdf.

[12] A. Adler, A. Bar-Gill, and N. Shimkin, "Optimal flight path for engine-out emergency landing," in *24th Control and Decision Conference*, IEEE, 2012.

[13] P. Eng, L. Mejias, X. Liu, and R. Walker, "Automating human thought processes for a UAV forced landing," *Journal of Intelligent and Robotic Systems: Theory and Applications*, vol. 57, no. 1-4, pp. 329–349, 2010, ISSN: 09210296. DOI: 10.1007/s10846-009-9389-8.

[14] P. Donato and E. Atkins, "Three-dimensional dubins path generation and following for a uas glider," in *Int. Con. on Unmanned Aircraft Systems*, Jun. 2017, pp. 294–303. DOI: 10.1109/ICUAS.2017.7991505.

[15] M. Warren, L. Mejias, J. Kok, X. Yang, F. Gonzalez, and B. Upcroft, "An automated emergency landing system for fixed-wing aircraft: Planning and control," *Journal of Field Robotics*, vol. 32, no. 8, pp. 1114–1140, 2015, ISSN: 15564967. DOI: 10.1002/rob.21641. [Online]. Available: http://eprints.qut.edu.au/89744/1/JFR%7B%5C_%7D2015.pdf.

[16] M. Coombes, W.-H. Chen, and P. Render, "Reachability Analysis of Landing Sites for Forced Landing of a UAS in Wind using Trochoidal Turn Paths," *Journal of Intelligent and Robotic Systems*, vol. 73, no. 1-4, pp. 635–653, 2015, ISSN: 0921-0296. DOI: 10.1007/s10846-013-9920-9. [Online]. Available: http://link.springer.com/10.1007/s10846-013-9920-9.

[17] S. Schopferer and T. Pfeifer, "Performance-aware flight path planning for unmanned aircraft in uniform wind fields," *Int. Conf. on Unmanned Aircraft Systems*, pp. 1138–1147, 2015. DOI: 10.1109/ICUAS.2015.7152406.

[18] S. Izuta and M. Takahashi, "Path Planning to Improve Reachability in a Forced Landing," *Journal of Intelligent and Robotic Systems*, vol. 86, no. 2, pp. 291–307, 2017, ISSN: 0921-0296. DOI: 10.1007/s10846-016-0431-3. [Online]. Available: http://link.springer.com/10.1007/s10846-016-0431-3.

[19] T. McGee, S. Spry, and J. Hedrick, "Optimal path planning in a constant wind with a bounded turning rate," *AIAA Guidance, Navigation, and Control Conference*, pp. 1–11, 2005.